

# Ultrafast Momentum Imaging of Chiral Interband Excitations in Graphene

S. Aeschlimann,<sup>1,\*</sup> R. Krause,<sup>1</sup> M. Chávez-Cervantes,<sup>1</sup> H. Bromberger,<sup>1</sup>  
A. Al-Temimy,<sup>2</sup> C. Coletti,<sup>2</sup> A. Cavalleri,<sup>1,3</sup> and I. Gierz<sup>1,†</sup>

<sup>1</sup>*Max Planck Institute for the Structure and Dynamics of Matter,  
Center for Free Electron Laser Science, Hamburg, Germany*

<sup>2</sup>*Center for Nanotechnology @ NEST,  
Istituto Italiano di Tecnologia, Pisa, Italy*

<sup>3</sup>*Department of Physics, Clarendon Laboratory,  
University of Oxford, Oxford, United Kingdom*

(Dated: January 24, 2017)

## Abstract

The chiral character of Dirac electrons in graphene manifests itself in a peculiar momentum anisotropy for photo-excited electron-hole pairs. These interband excitations are in fact forbidden along the direction of the light polarization, and are maximum perpendicular to it. This phenomenon gives rise to unconventional hot carrier dynamics that are only partially understood. Here, we use time- and angle-resolved photoemission spectroscopy to investigate the non-thermal physics of such chiral excitations, sampling carrier distributions as a function of energy and in-plane momentum. We first show that the rapidly-established quasi-thermal electron distribution initially exhibits an azimuth-dependent temperature, consistent with relaxation through collinear electron-electron scattering. Azimuthal thermalization is found to occur only at longer time delays, at a rate that is dependent on the type of static doping. In n-doped graphene, for which photo-excited carriers are generated close to the Fermi level, the anisotropy of the carrier temperature survives far longer than in p-doped graphene. We attribute this to the strong suppression of azimuthal relaxation due to a reduced phase space for optical phonon emission in the n-doped case. These experiments clarify new aspects of hot carrier dynamics that are unique to Dirac materials, with relevance for photo-control experiments and optoelectronic device applications.

The existence of anisotropic photo-carrier distributions in graphene was predicted [1, 2] and observed in optical pump-probe experiments [3–6], which showed a pronounced difference in the time-dependent optical response for different probe polarizations. The decay of the anisotropy extracted in this manner was attributed to optical phonon emission [2–5, 7, 8]. However, a complete picture for these non-equilibrium phenomena can only be obtained by tracking both carrier energy and momentum in the time domain.

Here we use time- and angle-resolved photoemission spectroscopy (tr-ARPES) at extreme ultraviolet (XUV) wavelengths to track the temporal evolution of the photo-excited carrier distribution as a function of energy and momentum. We establish a hierarchy of events that redistribute carriers on the Dirac cone, including the formation of an anisotropic, azimuth-dependent, electron temperature, which indicates that primary thermalization occurs through collinear electron-electron scattering. Azimuthal relaxation through optical phonon emission plays a role only at later time delays, and is strongly dependent on the type of static doping of the sample.

Two different kinds of graphene samples were used for the present investigation. N-doped monolayer samples were obtained by thermal decomposition of the silicon face of SiC, yielding an equilibrium chemical potential of  $\mu_e = +0.4$  eV [9, 10]. P-doped samples with the chemical potential at  $\mu_e = -0.2$  eV were instead obtained by decoupling the first inactive carbon monolayer formed by thermal decomposition of the same SiC face by hydrogen intercalation [10, 11]. After growth, these samples were exposed to air, characterized by Raman spectroscopy, reinserted into ultrahigh vacuum, and cleaned via annealing at 800°C.

The tr-XUV-ARPES experiments were performed at the MPISD in Hamburg. A Titanium:Sapphire amplifier operating at 1 kHz repetition rate was used to generate synchronized 800nm optical pump and XUV probe pulses. The latter were obtained by high harmonic generation in an Argon gas jet. The 17th harmonic at  $\hbar\omega_{\text{probe}} = 26.3$  eV was selected with a time-preserving grating monochromator [12] and used to measure photoelectron distributions from the sample. The probe polarization was fixed along the x axis (Fig. 1a). The polarization of the pump pulses was switched between x and y by rotating a half-wave plate. Both pump and probe impinged onto the sample at normal incidence. The experimental data shown in this work was obtained with a pump fluence of 2.8 mJ/cm<sup>2</sup>.

For the experiments reported here, we used a hemispherical analyzer with the entrance slit parallel to the x axis, to measure the photocurrent as a function of energy and in-plane

momentum  $k_x$  (Fig. 1a). In order to record the complete Dirac cone (photocurrent as a function of  $k_x$ ,  $k_y$ , and energy) we rotated the sample around the x axis.

Pump pulses at  $\hbar\omega_{\text{pump}} = 1.5 \text{ eV}$  generated electron-hole pairs at  $E_D \pm \hbar\omega_{\text{pump}}/2$ , where  $E_D$  is the energy of the Dirac point where conduction and valence band meet (Fig. 1b). This process mapped valence band states onto conduction band states of opposite chirality and pseudospin. Hence, optical excitation involved pseudospin flips which resulted in an angle-dependent transition probability  $|M_{\text{pump}}|^2 \propto \sin^2(\phi_k - \phi_A^{\text{pump}})$  [1, 2], where  $\phi_k$  and  $\phi_A^{\text{pump}}$  are the angles between the k-vector of the electron or the pump polarization and the x axis, respectively. As immediately evident from the expression above, the transition probability was then zero along the direction of the electric field ( $\phi_k = \phi_A^{\text{pump}}$ ) and maximum perpendicular to it.

Note also that the photocurrent is subject to momentum-dependent matrix element effects. The photoemission cross section in graphene is proportional to  $|M_{\text{probe}}|^2 \propto 1/2(1 + \cos(\phi_k - 2\phi_A^{\text{probe}}))$  [13–15], with  $\phi_A^{\text{probe}} = 0$  in the present experiment, which turns part of the Dirac cone invisible. The photoelectron distribution can then be obtained by multiplying the actual carrier distribution with  $|M_{\text{probe}}|^2$ .

Figures 1c-e illustrate the expected photoelectron distribution at  $E_D + \hbar\omega_{\text{pump}}/2$  as a function of  $k_x$  and  $k_y$  for excitation with x- and y-polarized light (Figs. 1a and b), and, for comparison, for a homogeneous carrier distribution (Fig. 1c). Figure 1f shows the expected evolution in time of the photocurrent inside the red box in Figs. 1c-e [2–8]. For pump pulses polarized along the x axis, the carriers are expected to fill these states only after scattering around the cone. Hence, we expect to measure a delayed rise and a lower peak signal for excitation with x-polarized light compared to excitation with y-polarized light. We also expect the two curves to overlap after thermalization, before further cooling by optical and acoustic phonon emission occurs at longer time delays [16–24].

In a first set of experiments we measured the photocurrent as a function of energy and  $k_x$ , and compared the effect of x- and y-polarized excitation in p- and n-doped samples (upper and lower panel of Fig. 2, respectively). Figures 2a and d show ARPES snapshots at a negative pump-probe delay and pump-induced changes of the photocurrent at the pump-probe delay at which the signal was maximum. In order to compare the number of excited carriers for x- and y-polarized pump pulses we integrated the photocurrent over the area indicated in Figs. 2a and d (white boxes). The time-dependent photocurrent is shown in

Figs. 2b and e. These data were fitted with an error function and a double exponential decay. We also show the temporal cross-correlation between pump and probe pulses (gray-shaded area), as obtained from the temporal derivative of the error function, with a full width at half maximum of 145 fs. For p-doped samples, the pump-probe signal for x- and y-polarized pump pulses was found to be the same within the error bars. On the contrary, we found a pronounced difference between the two pump polarizations for the n-doped sample, indicating the presence of a long-lived anisotropic carrier distribution. In Figs. 2c and f we plot the time-dependent anisotropy (difference between the dark and light blue curves in Figs. 2b and e), which was found to relax at a rate limited by the time resolution of the experiment.

Time-dependent carrier distributions for all  $k_x$  and  $k_y$  values were measured for n-doped samples and x-polarized pump pulses. Constant-energy cuts integrated over an interval of  $\pm 50$  meV around  $E_D + \hbar\omega_{\text{pump}}/2$  are reported for four different delays (Fig. 3), indicated by red arrows in Fig. 2e. At negative delay ( $t = -250$  fs) no excited carriers are detected. For time delays  $t = -25$  fs, that is half way through the rising edge, the anisotropic carrier distribution is already observable, reaching its maximum at  $t = +60$  fs. At  $t = +175$  fs the carrier distribution becomes isotropic, with an angular dependence caused by the photoemission matrix element alone. The measured spectra nicely agree with the expectations shown in Figs. 1c-e.

By integrating the two-dimensional ARPES spectra in Fig. 2d along  $k_x$  for x- and y-polarized pump pulses, we obtained transient electron distribution functions [25, 26] at the minima and maxima of  $|M_{\text{pump}}|^2$ , respectively, in the direction where the photoemission cross section is maximum. The gray data points in Fig. 4a show the distribution at negative delay. Light and dark orange data points show the distributions for x- and y-polarized pump pulses at  $t = +50$  fs where the pump-probe signal reaches its maximum for excitation with y-polarized light. The black lines are Fermi-Dirac fits convolved with a Gaussian with a full width at half maximum of 350 meV to account for the finite energy resolution. The temporal evolution of the resulting electron temperature is shown in Fig. 4b. At early times, the electron temperature along  $k_x$  is found to be smaller for x-polarized pump pulses than for y-polarized pump pulses.

We first note that the electron distribution can be described with a Fermi-Dirac distribution at all pump-probe delays (Fig. 4a), indicating that electron-electron scattering

thermalizes the photo-excited carriers on a time scale short compared to our temporal resolution. The observed pump-polarization dependence of the electron temperature (Fig. 4b) is equivalent to an azimuth dependence for excitation with a single pump polarization. This shows that electron-electron scattering is confined to lines pointing radially away from the Dirac point, as predicted in [2, 7].

Relaxation around the cone, which re-establishes an isotropic carrier distribution with azimuth-independent electron temperature (Fig. 3), is consistent with relaxation through optical phonon emission at  $\hbar\Omega_{\text{ph}} \approx 200$  meV [2–5, 7, 8]. However, phonon emission is only efficient if the excess energy of the excited electrons  $E - E_F$  is larger than the phonon energy  $\hbar\Omega_{\text{ph}}$  (Fig. 5). For the n-doped sample the initial excess energy  $\hbar\omega_{\text{pump}}/2 - E_F$  is far smaller than in the p-doped sample (0.35 and 0.95 eV, respectively). This results in a strong suppression of optical phonon emission and, hence, a longer lifetime of the carrier anisotropy. As the measured lifetime of the anisotropy in the present work is resolution limited, the difference in lifetime shows up as a difference in amplitude of the measured anisotropy (Fig. 2). A related suppression of optical phonon emission has been achieved by photo-excitation at small photon energies and small fluences in undoped samples [6].

In summary, we have used time- and angle-resolved photoemission spectroscopy to visualize anisotropic photo-carrier distributions in p- and n-doped monolayer graphene. We found that collinear electron-electron scattering rapidly thermalizes the carriers along lines pointing radially away from the Dirac point, leading to an azimuth-dependent electron temperature. We also observed a pronounced doping dependence of the lifetime of the carrier anisotropy. The close proximity between the energy of the photo-excited carriers and the equilibrium chemical potential in the n-doped sample efficiently reduces the emission rate of optical phonons and results in longer lifetimes of the anisotropic carrier distribution compared to the p-doped sample. These results visualize photo-carrier dynamics that are unique to Dirac materials, in which chiral carriers are responsible for peculiar anisotropic photo-carrier distributions. We also note that the ability to tune hot carrier dynamics via doping or gating might potentially be exploited in graphene-based thermoelectric devices [27–31], or other opto-electronic applications of this class of solids.

This work received financial support from the German Research Foundation through the Priority Program SPP1459 and the Collaborative Research Center SFB925 as well as the European Unions Horizon 2020 Research and Innovation Programme under Grant Agreement

---

\* Electronic address: sven.aeschlimann@mpsd.mpg.de

† Electronic address: isabella.gierz@mpsd.mpg.de

- [1] M. Trushin and J. Schliemann, *Europhys. Lett.* **96**, 37006 (2011)
- [2] E. Malic, T. Winzer, E. Bobkin, and A. Knorr, *Phys. Rev. B* **84**, 205406 (2011)
- [3] M. Mittendorff, T. Winzer, E. Malic, A. Knorr, C. Berger, W. A. de Heer, H. Schneider, M. Helm, and S. Winnerl, *Nano Lett.* **14**, 1504 (2014)
- [4] X.-Q. Yan, J. Yao, Z.-B. Liu, X. Zhao, X.-D. Chen, C. Gao, W. Xin, Y. Chen, and J.-G. Tian, *Phys. Rev. B* **90**, 134308 (2014)
- [5] M. Trushin, A. Grupp, G. Soavi, A. Budweg, D. De Fazio, U. Sassi, A. Lombardo, A. C. Ferrari, W. Belzig, A. Leitenstorfer, and D. Brida, *Phys. Rev. B* **92**, 165429 (2015)
- [6] J. C. König-Otto, M. Mittendorff, T. Winzer, F. Kadi, E. Malic, A. Knorr, C. Berger, W. A. de Heer, A. Pashkin, H. Schneider, M. Helm, and S. Winnerl, *Phys. Rev. Lett.* **117**, 087401 (2016)
- [7] E. Malic, T. Winzer, and A. Knorr, *Appl. Phys. Lett.* **101**, 213110 (2012)
- [8] A. Satou, V. Ryzhii, and T. Otsuji, *J. Phys. Conf. Ser.* **584**, 012018 (2015)
- [9] A. J. Van Bommel, J. E. Crombeen, and A. Van Tooren, *Surf. Sci.* **48**, 463 (1975)
- [10] U. Starke, S. Forti, K.V. Emtsev, C. Coletti, *MRS Bull.* **37** (12), 1177 (2012)
- [11] C. Riedl, C. Coletti, T. Iwasaki, A. A. Zakharov, and U. Starke, *Phys. Rev. Lett.* **103**, 246804 (2009)
- [12] F. Frassetto, C. Cacho, C. A. Froud, I. C. E. Turcu, P. Villorresi, W. A. Bryan, E. Springate, and L. Poletto, *Opt. Express* **19**, 19169 (2011)
- [13] E. L. Shirley, L. J. Terminello, A. Santoni, and F. J. Himpsel, *Phys. Rev. B* **51**, 13614 (1995)
- [14] H. Daimon, S. Imada, H. Nishimoto, and S. Suga, *J. Electron. Spectrosc. Relat. Phenom.* **76**, 487 (1995)
- [15] A. Bostwick, T. Ohta, J. L. McChesney, K. V Emtsev, T. Seyller, K. Horn, and E. Rotenberg, *New J. Phys.* **9**, 385 (2007)
- [16] J. C. Johannsen, S. Ulstrup, F. Cilento, A. Crepaldi, M. Zacchigna, C. Cacho, I. C. E. Turcu, E. Springate, F. Fromm, C. Raidel, T. Seyller, F. Parmigiani, M. Gioni, and P. Hofmann,

- Phys. Rev. Lett. 111, 027403 (2013)
- [17] M. Breusing, S. Kuehn, T. Winzer, E. Malic, F. Milde, N. Severin, J. P. Rabe, C. Ropers, A. Knorr, and T. Elsaesser, Phys. Rev. B 83, 153410 (2011)
- [18] T. Kampfrath, L. Perfetti, F. Schapper, C. Frischkorn, and M. Wolf, Phys. Rev. Lett. 95, 187403 (2005)
- [19] H. Yan, D. Song, K. F. Mak, I. Chatzakis, J. Maultzsch, and T. F. Heinz, Phys. Rev. B 80, 121403 (2009)
- [20] K. Kang, D. Abdula, D. G. Cahill, and M. Shim, Phys. Rev. B 81, 165405 (2010)
- [21] T. Winzer, A. Knorr, and E. Malic, Nano Lett. 10, 4839 (2010)
- [22] J. C. W. Song, M. Y. Reizer, and L. S. Levitov, Phys. Rev. Lett. 109, 106602 (2012)
- [23] M. W. Graham, S.-F. Shi, D. C. Ralph, J. Park, and P. L. McEuen, Nat. Phys. 9, 103 (2013)
- [24] A. C. Betz, S. H. Jhang, E. Pallecchi, R. Ferreira, G. Fve, J.-M. Berroir and B. Plaças, Nat. Phys. 9, 109 (2013)
- [25] I. Gierz, J. C. Petersen, M. Mitrano, C. Cacho, I. C. E. Turcu, E. Springate, A. Stöhr, A. Köhler, U. Starke, and A. Cavalleri, Nat. Mater. 12, 1119 (2013)
- [26] S. Ulstrup, J. C. Johannsen, M. Grioni, and P. Hofmann, Rev. Sci. Instrum. 85, 013907 (2014)
- [27] T. Mueller, F. Xia, and P. Avouris, Nat. Photonics 4, 297 (2010)
- [28] F. Bonaccorso, Z. Sun, T. Hasan and A. C. Ferrari, Nat. Photonics 4, 611 (2010)
- [29] N. M. Gabor, J. C. W. Song, Q. Ma, N. L. Nair, T. Taychatanapat, K. Watanabe, T. Taniguchi, L. S. Levitov, P. Jarillo-Herrero, Science 334, 648 (2011)
- [30] D. Sun, G. Aivazian, A. M. Jones, J. S. Ross, W. Yao, D. Cobden, and X. Xu, Nat. Nanotechnol. 7, 114 (2012)
- [31] T. J. Echtermeyer, P. S. Nene, M. Trushin, R. V. Gorbachev, A. L. Eiden, S. Milana, Z. Sun, J. Schliemann, E. Lidorikis, K. S. Novoselov, and A. C. Ferrari, Nano Lett. 14, 3733 (2014)

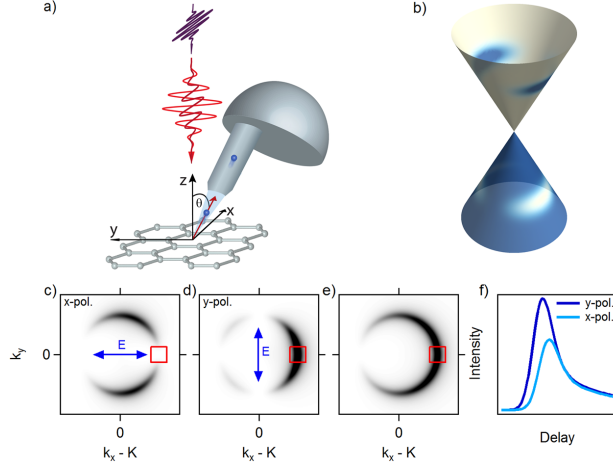


FIG. 1: a) Sketch of the experimental setup. The sample is excited with x- or y-polarized pump pulses (red). Photoelectrons are ejected with x-polarized XUV probe pulses (violet) and pass through a hemispherical analyzer. b) Expected anisotropic charge carrier distribution after photo-excitation of monolayer graphene. Occupied and empty states are shown in blue and white, respectively. c)-e) Expected photoemission spectra at constant energy  $E = E_D + \hbar\omega_{\text{pump}}/2$  as a function of  $k_x$  and  $k_y$  in the first instant after photo-excitation with x- (c) and y-polarized light (d) and the expected spectrum of an isotropic distribution (e). f) Sketch of the expected temporal evolution of the number of carriers inside the red box shown in (c), (d) and (e).



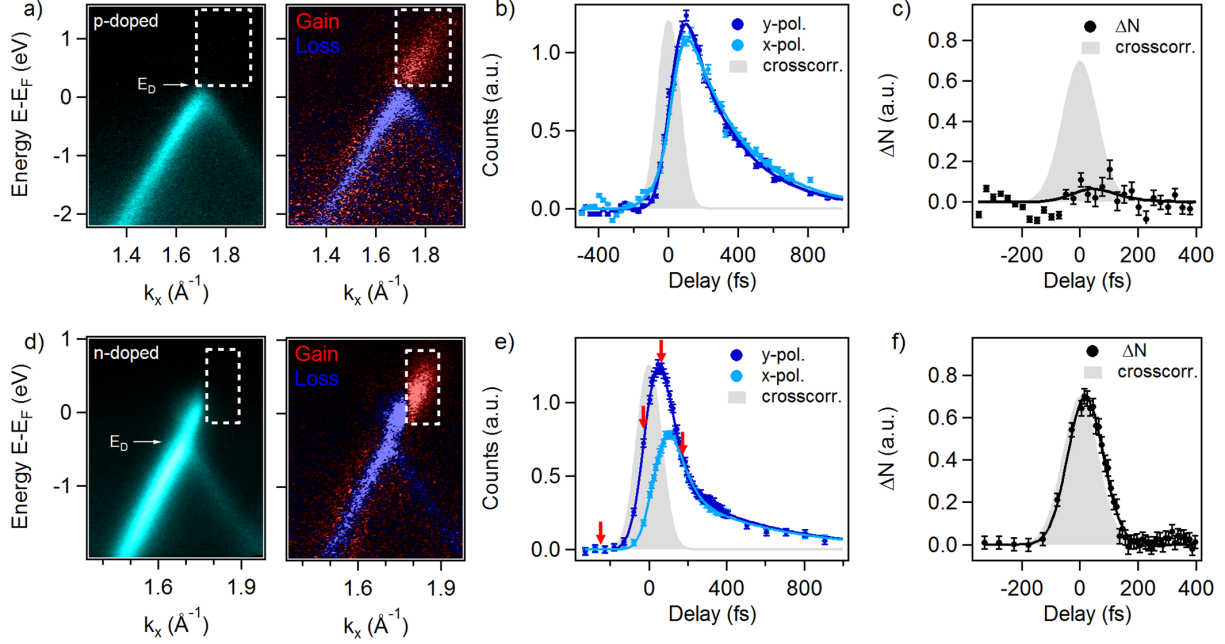


FIG. 2: Photoemission data for p-doped (upper panel) and n-doped graphene (lower panel): a), d) ARPES spectra for negative time delays and pump-induced changes of the photocurrent for y-polarized pump pulses at the peak of the pump-probe signal. b), e) photocurrent integrated over the area of the white boxes in (a) and (d) versus pump-probe delay for x- (light blue) and y-polarized pump pulses (dark blue). The respective difference in intensity is shown in (c) and (f). The light gray area represents the temporal cross-correlation of pump and probe pulses.

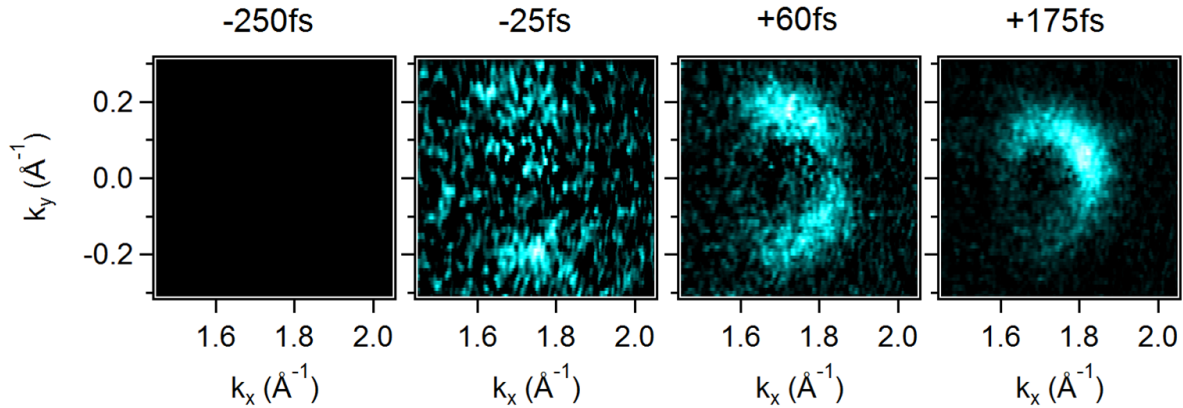


FIG. 3: Photoemission spectra at constant energy  $E = E_D + \hbar\omega_{\text{pump}}/2$  as a function of  $k_x$  and  $k_y$  at four different time delays as indicated by red arrows in Fig. 2e. Note: The sickle-shaped image at  $t = 175$  fs is slightly rotated away from the  $k_x$  axis due to a small azimuthal misalignment of the sample.

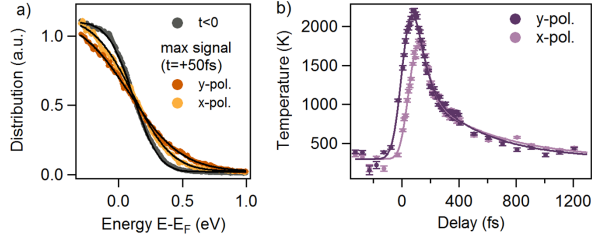


FIG. 4: a) electron distribution functions along the  $k_x$  direction for n-doped graphene. Gray curves show the distribution at negative pump-probe delay, light and dark orange curves show the respective distributions at  $t = 50$  fs for x- and y-polarized pump pulses. Black curves are Fermi-Dirac fits. b) Temporal evolution of the electron temperature obtained from the fits in (a).

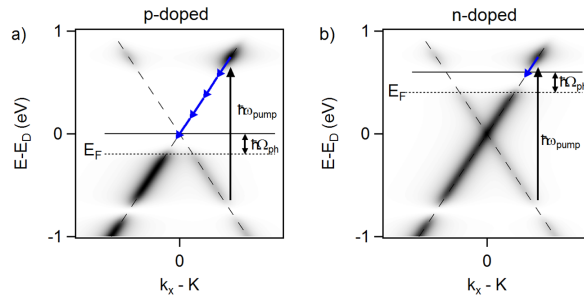


FIG. 5: Sketch of photo-excited carrier distributions for p- (a) and n-doped graphene (b). Electrons with energies between  $E_F$  and  $E_F + \hbar\Omega_{ph}$  cannot emit phonons due to Pauli blocking. The reduced phase space results in a strong suppression of optical phonon emission in n-doped graphene.